Journal of Computational Physics 228 (2009) 2282–2295

Contents lists available at ScienceDirect

Journal of Computational Physics

journal homepage: www.elsevier.com/locate/jcp

Finite difference time domain algorithm for electromagnetic problems involving material movement

C.D. Sijoy *, Shashank Chaturvedi

Computational Analysis Division, Bhabha Atomic Research Centre, Trombay, Mumbai, India

ARTICLE INFO

Article history:
Received 25 July 2008
Received in revised form 4 December 2008
Accepted 4 December 2008
Available online 24 December 2008

PACS:
82.20.Wt
03.50.De

Keywords:
FDTD
Electromagnetic induction
Magnetic diffusion
Magnetic flux compression
Parallel computation
Variable mesh
Material movement
Motional emf

ABSTRACT

The finite difference time domain (FDTD) method, adapted for magnetic field diffusion problems, is used to study the electromagnetic induction in moving materials by including motional emf in standard FDTD electromagnetic equations. The material movement is implemented by continuously changing material properties in each computational cell consistent to material advection. The flux corrected transport (FCT) algorithm is used to transport magnetic field in a fixed eulerian cell. A higher time-step is achieved by artificially increasing permittivity of the medium. This new approach is validated with standard analytical solutions for planar magnetic flux compression system and magnetic field diffusion in moving conductors with a non-relativistic velocity. To our knowledge, this is the first approach to use FDTD method for electromagnetic problems involving material motion.

1. Introduction

Magnetic flux compression systems [1] are in widespread use for generating megagauss magnetic fields for a variety of applications. Numerical simulations for such systems can involve complex geometries as well as multiple materials like conductors, dielectrics and plasma. More importantly, these systems involve material motion in the presence of intense magnetic fields. These simulations rely on accurate calculation of the penetration of electromagnetic fields through moving conductors. Such a calculation yields the spatio-temporal evolution of electromagnetic fields, along with lumped parameters like the time-dependent resistance and inductance.

One commonly-used method is to solve the magnetic field diffusion equation [2]. However, the electrical conductivity, and hence the magnetic field diffusion coefficient, can vary by orders of magnitude in space and time. This leads to numerical problems, requiring a near-zero time-step. The problem is further complicated by imperfectly-known boundary conditions for the magnetic field. Another difficulty in magneto-hydrodynamic (MHD) calculations for such systems is the self-consistent coupling of external circuit equations to hydrodynamic calculations via the current density [2].

* Corresponding author. Tel.: +91 7923962114; fax: +91 792392277.
E-mail address: cjoy_davis@yahoo.co.in (C.D. Sijoy).

0021-9991/$ - see front matter © 2008 Elsevier Inc. All rights reserved.
doi:10.1016/j.jcp.2008.12.008

Analytical treatments of magnetic field diffusion in such systems are only possible for simple geometries, e.g., slab geometry [3–5]. To our knowledge, none of the closed-form expressions can handle all the complexities listed above.

Earlier works by Holland in [8], have explored the capability of finite difference time domain (FDTD) method [6,7] for calculating magnetic field diffusion into a cavity created by conducting wall when exposed to incident electromagnetic wave. Higher time-step is achieved by artificially increasing permittivity of the medium. Similarly in [9], a reduced velocity of light approach is used for the analysis of Nonlinear magnetic field diffusion using FDTD method in three-dimensions for static conductors. However, those calculations were limited to static conductors exposed to external incident electromagnetic wave. Magnetic flux compression systems involve field diffusion in to a moving conductor.

There is thus a need for a more general method that can handle real-life problems with all the complexities listed earlier. The finite difference time domain (FDTD) method for electromagnetics is one such method. This method directly updates Maxwell's curl equations in time, using an explicit algorithm, to yield the spatio-temporal variation of electric and magnetic fields [6,7]. It allows setting up of complex, multi-material configurations. Furthermore, the time domain analysis allows handling of arbitrary time-dependent waveforms of current. This technique thus allows a study of real-life configurations with practically no limitations on the geometric complexity, the materials used or the temporal waveforms.

A detailed description of the application of FDTD method for such systems and its advantage over conventional methods is available in our earlier work [11–13]. Those studies were, however, limited to static conductors.

In the present study, we have included velocity-dependent electromagnetic induction terms in the FDTD equations. A leapfrog method [7] is used to update electric and magnetic fields, and a Flux Corrected Transport (FCT) algorithm [14,15] is used for magnetic field transport. This new method can be used for electromagnetic problems involving material movement.

In the present work, we report details of this modified FDTD method for electromagnetic problems involving material movement, related issues and its validation. We restrict our calculations to two spatial dimensions (2D), although its three dimensional (3D) implementation is straightforward. To our knowledge, this is the first application of this powerful technique to systems involving material movement.

2. Method and important issues

2.1. Algorithm

The past decade has seen rapidly-increasing growth of the finite difference time domain method to calculate scattering and absorption of electromagnetic waves from lossy dielectrics as well as conducting objects [16–18]. The FDTD method is an explicit time domain approach for solving Maxwell's curl equations. For problems involving static conductors, these equations can be written

$$\nabla \times \vec{E} = -\mu \frac{\partial \vec{H}}{\partial t} \tag{1}$$

$$\nabla \times \vec{H} = \varepsilon \frac{\partial \vec{E}}{\partial t} + \sigma \vec{E} \tag{2}$$

on spatial grids, based on a technique introduced by Yee [7]. Here, $\vec{E}$ and $\vec{H}$ represent the electric field and magnetic field intensities, respectively, while σ, μ and ε represent the electrical conductivity, magnetic permeability and permittivity respectively. The finite difference equations are stepped in time, alternately updating the $\vec{E}$ and $\vec{H}$ components at each grid point. A typical Yee cell in 3D, and the corresponding locations of different field components, is shown in Fig. 1.

The object to be modeled is set up in a Cartesian computational grid with mesh sizes of Δx, Δy and Δz in the x-, y- and z-directions, respectively. The time-step is governed by the Courant criterion for speed-of-light transit through the smallest computational cell and it is calculated using Eq. (3) [6,7]

$$\Delta t = \frac{1}{c\sqrt{\frac{1}{\Delta x^2} + \frac{1}{\Delta y^2} + \frac{1}{\Delta z^2}}} \tag{3}$$

where $c = 1/\sqrt{\mu\epsilon}$ is the velocity of light.

For problems of our interest, involving magnetic field diffusion, the standard finite difference form used in FDTD [6,7] is not suitable. It has been suggested in [20,21] that exponential time differencing (ETD) be used in finite difference time domain implementation in high conductivity regions were large dissipation exists. This suggestion is based on the belief that ETD permits $\sigma\Delta t/\epsilon \gg 1$, while maintaining accuracy in those regions. The $\sigma\Delta t/\epsilon \gg 1$ condition arises from the fact that the time-step involved should resolve the conduction current relaxation timescales. More details can be found in [22].

Hence the standard scheme is replaced by an explicit exponentially-differenced form, to avoid the possibility of diffusion instability [19,9,10]

$$E_x^{n+\frac{1}{2}} = e^{\frac{-\sigma\Delta t}{\epsilon}} E_x^{n-\frac{1}{2}} + \left[\frac{1 - e^{\frac{-\sigma\Delta t}{\epsilon}}}{\sigma}\right] (\nabla \times \vec{H})_x^n \tag{4}$$

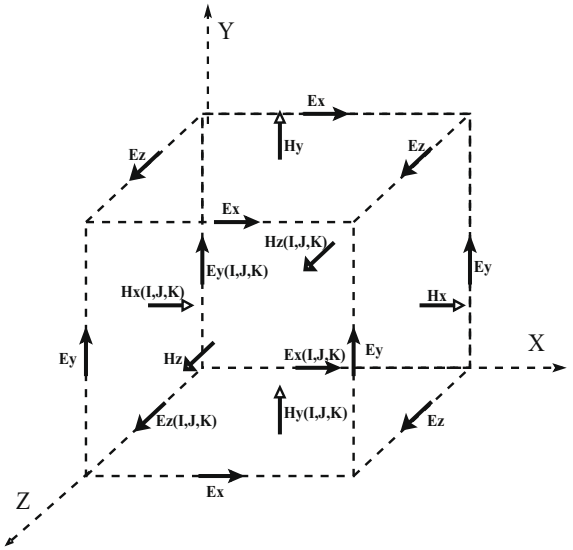

Fig. 1. Yee cell with electric and magnetic field locations.

where superscript '*n*' is the time index and subscript *x* denotes the *x*-component of a vector. Other components of $\vec{E}$ follow similar relations. This modification increases computational accuracy in the presence of dissipation. This scheme reduces to a standard differencing form when $\sigma\Delta t/\epsilon \ll 1$, so that $e^{-\sigma\Delta t/\epsilon} \approx 1 - \sigma\Delta t/\epsilon$. This approach allows handling of large values of σ. A more detailed analysis of exponential time differencing for FDTD in lossy dielectrics is given in [22].

Let us now consider problems involving magnetic field diffusion through moving conductors. We limit ourselves to non-relativistic cases, which is sufficient for practical systems such as magnetic flux compression systems. Hence the effect on displacement current can be neglected. The motion of a conductor in an external magnetic field can create an electric field or voltage (motional emf) that can induce a flow of current in the conductor. This can be expressed mathematically by the relation

$$\vec{E}' = \vec{E} + \vec{v} \times \vec{B} \tag{5}$$

The conduction current density $\vec{J}$, which was written as $\sigma\vec{E}$ in Eq. (2), must now include the motional emf

$$\vec{J} = \sigma[\vec{E} + \vec{v} \times \vec{B}]$$

where $\vec{B} = \mu\vec{H}$. This corresponds to a motional electric field, $\vec{E}_v = \mu(\vec{v} \times \vec{H})$, induced in materials having finite conductivity and velocity.

For most problems in time-dependent field problems, where currents are induced by non-relativistic velocities, $\vec{D}' \approx \vec{D}$ and $\vec{B}' \approx \vec{B}$, (see, e.g., [34,23]). Thus, the electric field and hence conduction current density will be the only variables that differes significantly.

We have examined two different methods of adding $\vec{E}_v$ term, which are explained below. The relevant theories followed and its mathematical formulations can be found in [24].

2.1.1. Scheme-1

One way of adding this motional electric field term is described below:

Calculate total electric field, $\vec{E}' = \vec{E} + \vec{v} \times \vec{B}$. Now, update electric field using Eq. (6) which include the $\vec{v} \times \vec{B}$ term

$$\frac{\partial \vec{E}}{\partial t} = -\frac{\nabla \times \vec{H}}{\varepsilon} + \frac{\sigma}{\varepsilon}\vec{E}' \tag{6}$$

The magnetic field can be updated using Eq. (7)

$$\frac{\partial \vec{H}}{\partial t} = -\frac{\nabla \times \vec{E}}{\mu} \tag{7}$$

We found that the results obtained using this scheme is leads to ripples in numerical solutions, which will be discussed in later sections.

2.1.2. Scheme-2

The ripple problem can be removed by using special algorithms like the total variation diminishing (TVD) scheme [25–27] or the method of characteristics (MOC) [28]. A comparative study on TVD scheme and the flux corrected transport (FCT) method can be found in [27], which also lists some advantages of the FCT algorithm over the TVD scheme. The FCT procedure adds higher order anti-diffusive terms to the stable but diffusive low-order solution and a limiter ensures that no new minima or maxima with respect to the low-order solution are created [14,15]. This method ensures a monotonic solution. A detailed discussion can be found in [14,15]. The FCT algorithm satisfies $\nabla \cdot \vec{H} = 0$ condition fairly accurately, limited only by round off errors. It is also efficient at resolving sharp spatial gradients. Finally, its implementation is simple. We have, therefore, opted to use the FCT algorithm to modify the standard FDTD equations for magnetic field diffusion through moving conductors.

We have added the motional electric field to Eq. (1). This leads to the following equation for magnetic field updation:

$$\frac{\partial \vec{H}}{\partial t} = -\frac{1}{\mu}\nabla \times \vec{E}' + \nabla \times \vec{v} \times \vec{H} \tag{8}$$

Applying some mathematical treatment, along with the condition $\nabla \cdot \vec{H} = 0$, the final form of Eq. (1) becomes

$$\frac{\partial \vec{H}}{\partial t} + \nabla \cdot (\vec{v}\vec{H}) = S_H \tag{9}$$

where $\nabla \cdot (\vec{v}\vec{H})_j = \Sigma_i \partial(v_i H_j)/\partial x_i$ in Cartesian coordinates. The source term S_H is given by

$$S_H = \nabla \cdot (\vec{H}\vec{v}) - \frac{1}{\mu}\nabla \times \vec{E}' \tag{10}$$

Eq. (9) is solved using the flux corrected transport (FCT) method. We have used a multi-dimensional flux limiter suggested in [29] and [30].

The electric field equation can be updated using the following equation which include $\vec{v} \times \vec{B}$ term:

$$\frac{\partial \vec{E}}{\partial t} = -\frac{\nabla \times \vec{H}}{\varepsilon} + \frac{\sigma}{\varepsilon}\vec{E}' \tag{11}$$

A variety of boundary conditions are available for FDTD algorithms [16]. It turns out that in the problems of interest here, the choice of boundary condition is not very critical, as long as the boundary is far from the the object through which magnetic field diffusion is taking place. Hence we have used Mur's second order outer radiation boundary condition (ORBC) [31,6]. For other problems, more appropriate boundary conditions could be used.

Due to material movement through the mesh, the electrical conductivity throughout the domain must be updated at every time-step. This is particularly critical at conductor–insulator interfaces, where the conductivity changes by orders of magnitude. The conductivity in each computational cell is calculated based on the mass density – details are given in Section 2.4. Hence it is necessary to evolve material density throughout the domain, given the spatio-temporal distribution of velocity. This is done using the continuity equation

$$\frac{\partial \rho}{\partial t} + \nabla \cdot (\vec{v}\rho) = 0 \tag{12}$$

where $\vec{v}$ is the material/conductor velocity. The velocity distribution in space and time, throughout the computational domain, must be externally specified. In the present study, the velocity distribution required throughout the domain in space and time are given as an input parameter. Updation of velocity consistent to the deceleration of the moving conductor by magnetic pressure lies beyond the scope of this work.

2.2. Important issues

In our previous work [11], we gave a detailed discussion of major issues that arise while using the FDTD method for solving magnetic diffusion problems for static conductors. A few important issues are summarized here for ready reference.

Firstly, the modeling of curved geometries, in a Cartesian grid, leads to "staircase" errors that must be minimized by using a sufficient number of cells [6]. Secondly, the cell size must not exceed 10% of the free-space wavelengths λ corresponding to the frequencies of interest [6]. Thirdly, since an ORBC is used, it is necessary to maintain a distance of at least 1–2 λ between the object and the domain boundary in all directions [6]. Fourthly, there must be a sufficient number of cells in one skin-depth, for proper resolution of the penetration of the magnetic field. Fifthly, the wavelength corresponding to the applied frequency should be very different from system dimensions, to eliminate the possibility of radiation, which would not be significant in a real-life system. These criteria, put together, lead to a rather large computational load.

This problem can be solved by using an artificially increased permittivity for the medium by a large factor, which reduces the speed of light and thereby permits much larger time-steps [9–11]. Since λ is proportional to the speed of light, the cell size required to resolve the wavelength becomes a few mm. Therefore, there is a great reduction in computational demand by increasing ϵ. However, the cell size required to resolve the skin-depth is 10–1000 times smaller, depending upon the conductivity and frequency. The only solution is to have variable meshing, which is constant through the conductor region, but expands in the free-space region surrounding the object.

Another issue is to ensure that the magnetic diffusion timescale in good conductors is not affected by the use of an artificially large permittivity to achieve higher time-steps in the simulation. The magnetic diffusion time in a conductor having thickness 'a' and conductivity σ is given by $t_d = \mu\sigma a^2$. This time scale will not be affected by increasing ϵ in the medium. However, the time-step used in the computation should not exceed the magnetic diffusion time scale and it should be able to resolve the magnetic diffusion time. In our simulations, we have scaled the permittivity keeping these constraints in mind. A detailed discussion on these issues and its solutions are mentioned in our previous work [11].

For effective magnetic flux compression, the quantity R_d, defined as the ratio of magnetic diffusion time to compression time, should satisfy Eq. (13). In our present study, the quantities which determines R_d are chosen in such a way that the overall computational requirement is minimized while satisfying Eq. (13).

Despite all these changes discussed above, due to the large number of constraints that have to be satisfied, the computational demand is too large to be handled on one CPU. Hence the computer code has been parallelized using message passing interface (MPI) [32] in all directions, with the flexibility to independently specify the number of sub-divisions in each direction.

2.3. Theoretical model for a simple system

This new method has been validated against analytical solutions for the spatio-temporal distribution of the magnetic field, given in [3–5]. These solutions apply to a simple flux compression system having the slab geometry shown in Fig. 2. The system consists of a slab with a finite conductivity σ and thickness a, placed inside two ideally conducting walls with infinite conductivity. The slab moves across a transverse magnetic field with a uniform velocity, v. B_{10} and B_{20} are the initial transverse (z-component) magnetic fields to the left and right of the conductor. In Fig. 2, L is the length of the 'compression volume'. As the slab moves to the right, it reduces L, leading to an amplification in the external magnetic field B_{20} by flux compression and a dilution of magnetic field B_{10} behind the slab [4,5].

The process involved are (a) the induction of electromagnetic fields in the conductor resulting from its motion across $B(x,t)$, and (b) diffusion of this magnetic field through the moving conductor, etc. [3–5]. The extent of field amplification depends on two competing effects. Diffusion of flux through the conductor reduces the total flux left in the compression volume. The remaining flux is compressed into a progressively smaller volume, leading to an increase in magnetic field. The efficiency of flux compression in the compression volume is related to a dimensionless number

$$R_d = \frac{\mu\sigma a^2 v}{L} \tag{13}$$

which is the ratio of the diffusion time $t_d = \mu\sigma a^2$ to the compression time $t_v = L/v$. The higher the value of R_d, the better is expected to be the conservation of flux in the compression volume.

This is an initial-boundary-value-problem (IBVP) and can be solved analytically as in [4,5]. The displacement current is neglected in [4,5] while deriving analytical solutions, since the electromagnetic field changes are produced by non-relativistic conductor motion. Also, the diffusion of electromagnetic field through the moving conductor is described by the linear parabolic diffusion equation, since joule heating is neglected for the present study. More details can be found in [4,5].

In order to remain consistent with[3–5], we have neglected the deceleration of the moving conductor and its compression due to magnetic pressure, which becomes significant at high fields. However, it is easy to include both effects in the FDTD calculation.

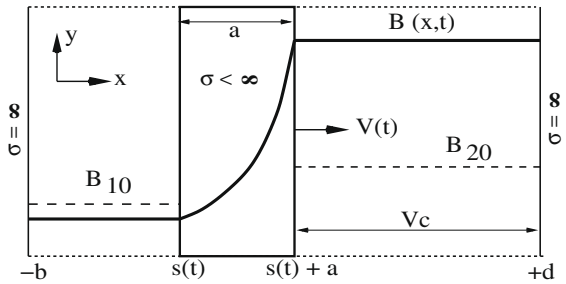

Fig. 2. Electromagnetic induction model with a moving conductor and fixed end conductors at $x = -b$ and $x = +d$. B_{10}, B_{20} are the initial transverse magnetic fields to the left and right of the conductor. The symbol V_c marks the 'compression volume'.

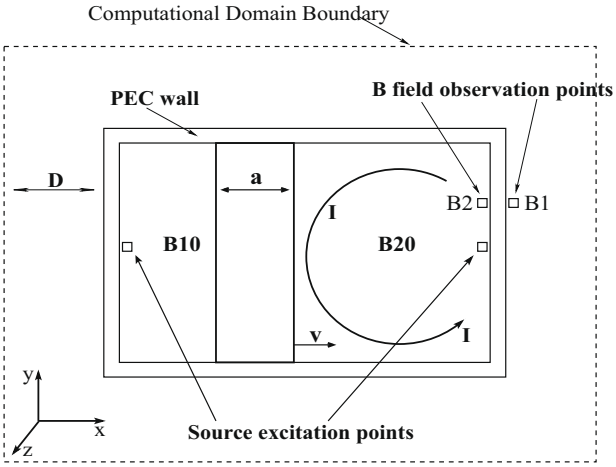

Fig. 3. FDTD setup, with source excitation points and magnetic field observation points (B_1 and B_2). D is the distance to computational boundary.

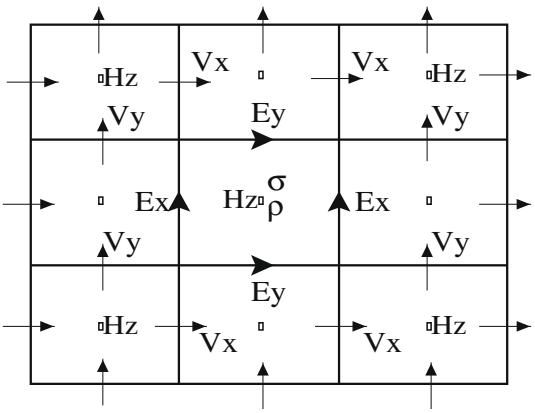

Fig. 4. Two-dimensional (2D) Yee cell, showing locations of field components and material quantities.

2.4. Computational model

The FDTD setup is as shown in Fig. 3. The object is modeled in a 2D Cartesian grid. For the present problem, only E_x and E_y components of the electric field and the H_z component of the magnetic field exists. The electric and magnetic field components are located according to a 2D Yee cell configuration, as shown in Fig. 4. Material quantities like conductivity, σ and density, ρ are specified at the center of a computational cell, while velocities are specified at the faces of the cell. The specification of field locations in this manner requires boundary conditions only for electric field components. In order to remain consistent with FCT algorithms [14,15], the velocities are specified on the edge faces.

The conductor, having a thickness a, is enclosed by a perfectly electrically conducting (PEC, $\sigma = \infty$) wall. Mur's outer radiation boundary condition (ORBC) [31,6] has been used to terminate the computational domain. In order to avoid unphysical reflections from the termination boundary due to ORBC, a minimum distance D must be maintained between the PEC wall and the computational boundary in all directions. D is typically 1–2 λ [6]. A gap of 20–40 cells has been found to be sufficient for the present problem.

For the present problem we found that no field get diffused through PEC wall and therefore the number of cells between the object (PEC wall) and the boundary can be reduced considerably. The initial magnetic fields B_{10} and B_{20} are specified analytically at two different source excitation points, see Fig. 3, with one computational cell for each source excitation point. The field observation points B_1 and B_2 are used for recording magnetic field at different time.

In the FDTD method, the highest frequency that can be handled is limited by the mesh-size. From stability considerations, the free-space wavelength λ corresponding to that frequency should not be smaller than four computational cells [6]. For reasonable accuracy, it is desirable to have at least 10 cells in one λ. Now, a step-change in any quantity contains all frequencies,

so it cannot be handled by any practical mesh-size. Hence it is not acceptable to start the simulation with a jump in B_1 and B_2 to their desired values B_{10} and B_{20}. Starting from zero values of all field components, a gradual increase becomes necessary. We have used a sinusoidal excitation function given by Eq. (14)

$$B_z = B_0 \sin(\omega t), \quad B_0 = B_{10}, B_{20}, \quad 0 < t < t_B \tag{14}$$

where t_B is the 0–100% rise-time of the magnetic field, corresponding to the quarter-wave time, when $\omega = 2\pi/(4t_B)$ is the angular frequency. This will fill up uniform magnetic fields B_{10} and B_{20} at the left and right side of the conductor respectively.

Apart from satisfying the stability criterion, the field rise-time for both source excitation points is determined in such a way that negligible diffusion takes place into the slab before the movement, so as to trap most of the flux between the conductor and PEC wall.

The conducting slab is held stationery until $t = t_B$, at which point is suddenly starts moving to the right with a constant specified velocity, compressing the initial magnetic field along the x-direction. The material density in each computational cell is evolved using Eq. (12). A multi-dimensional flux corrected transport (FCT) method is used for this purpose [29]. The material conductivity (σ^m) for material m in each computational cell is calculated using an approximate expression given by Eq. (15), which is based on the assumption that the material is uniformly filled in the entire region of the cell

$$\sigma^m(i,j) = \sigma_0^m \times \frac{\rho^m(i,j)}{\rho_0^m} \tag{15}$$

where ρ_0^m, $\rho^m(i,j)$ are the normal density of material 'm' and its instantaneous material density, respectively. Similarly σ_0^m, $\sigma^m(i,j)$ are electrical conductivities corresponds to normal density and instantaneous density, respectively. Here, cell indices i and j correspond to the x- and y-directions, respectively. The total conductivity in a computational cell is calculated using the weighted average of individual conductivities of all materials present in that cell, which can be expressed as in Eq. (16)

$$\sigma_T(i,j) = \frac{\sum_{m=1}^{M} \rho^m(i,j)\sigma^m(i,j)}{\sum_{m=1}^{M} \rho^m(i,j)} \tag{16}$$

where M is the total number of materials present in a cell.

Finally, the equations to be solved for the present problem in two dimensions can be summarized in finite difference form as below:

$$E_x^n(i,j) = E_x^{n-1}(i,j) + \frac{\Delta t}{\epsilon_0}\left[\frac{H_z^{n-\frac{1}{2}}(i,j) - H_z^{n-\frac{1}{2}}(i,j-1)}{\Delta y}\right] \tag{17}$$

$$E_y^n(i,j) = E_y^{n-1}(i,j) + \frac{\Delta t}{\epsilon_0}\left[\frac{H_z^{n-\frac{1}{2}}(i,j) - H_z^{n-\frac{1}{2}}(i-1,j)}{\Delta x}\right] \tag{18}$$

$$E_x^n(i,j) = E_x^{n-1}(i,j)e^{-\sigma(i,j)\Delta t/\epsilon(i,j)} + (1 - e^{-\sigma(i,j)\Delta t/\epsilon(i,j)}) \times \left[\frac{H_z^{n-\frac{1}{2}}(i,j) - H_z^{n-\frac{1}{2}}(i,j-1)}{\sigma(i,j)\Delta y} - \mu v_y(i,j)H_z(i,j)\right] \tag{19}$$

$$E_y^n(i,j) = E_y^{n-1}(i,j)e^{-\sigma(i,j)\Delta t/\epsilon(i,j)} + (1 - e^{-\sigma(i,j)\Delta t/\epsilon(i,j)}) \times \left[\frac{H_z^{n-\frac{1}{2}}(i,j) - H_z^{n-\frac{1}{2}}(i-1,j)}{\sigma(i,j)\Delta x} + \mu v_x(i,j)H_z(i,j)\right] \tag{20}$$

$$H_z^{n+\frac{1}{2}} = H_z^{n-\frac{1}{2}} - \frac{\Delta t}{\mu_0} \times \left[\frac{E_y^n(i+1,j) - E_y^n(i,j)}{\Delta x}\right] - \frac{\Delta t}{\mu_0} \times \left[\frac{E_x^n(i,j+1) - E_y^n(i,j)}{\Delta y}\right] - \frac{\partial F_x^{n+\frac{1}{2}}}{\partial x} - \frac{\partial F_y^{n+\frac{1}{2}}}{\partial y} \tag{21}$$

Here, Eqs. (17) and (18) are for free space, while Eqs. (19) and (20) are for lossy dielectrics. $F_x^{n+\frac{1}{2}} = v_x(i,j)H_z(i,j)$ and $F_y^{n+\frac{1}{2}} = v_y(i,j)H_z(i,j)$ are x-directed and y-directed fluxes evaluated at the faces of the Yee cell, using the FCT algorithm. n is the time index and i, j are the space indices. The conductivity values required at various electric field locations (cell faces) are obtained by taking the average of cell-centered conductivities surrounding that face.

The computational algorithm for Scheme-2 can be described as follows:

Initialize time, $t = 0$

(i) initialize E_x, E_y, H_z, ρ, σ, etc.

1. E update
   (i) Update electric fields using Eqs. (17)–(20)
   (ii) if $(t < t_B)$ then, apply source terms for electric fields, if any (This section will be used if one has an applied voltage excitation [11–13] rather than magnetic field excitation for establishing current flow in the system. For the present problem we have used magnetic field excitation)
   Advance time, $t = t + \frac{\Delta t}{2}$

2. H update
   (i) transport magnetic field using FCT; Eq. (9).
   (ii) if $(t < t_B)$ then, apply source terms for magnetic fields using Eq. (14). The source fields B_{10} and B_{20} are specified at two different excitation points with one computational cell for each. See Fig. 3. This will establish a current flow in the system.
   Advance time, $t = t + \frac{\Delta t}{2}$

3. Material movement at full time-step
(i) advect material using FCT; Eq. (12)
(ii) update conductivity in each cell using convected density; Eqs. (15) and (16).
If $t < t_{stop}$ go to step 1

4. Stop

Basic steps involved in the FCT algorithm are as follows:

1. Calculate and apply the convective and diffusive fluxes in x-direction
2. Calculate and apply the convective and diffusive fluxes in y-direction
3. Add source terms, if any
4. Calculate the anti-diffusive fluxes in x and y direction
5. Limit and apply correction factors to the anti-diffusive fluxes in x and y direction
6. Compute the solution

Details of each step and its evaluation schemes can be found in [14,15]. Multi-dimensional problems in FCT are solved by using directional splitting [14]. We have used a fully multi-dimensional flux limiter suggested in [29] and [30] for performing step 5 above, which does not require a directional splitting algorithm.

For the present problem, $\nabla \cdot \vec{H} = \left(\frac{\partial H_x}{\partial x} + \frac{\partial H_y}{\partial y} + \frac{\partial H_z}{\partial z}\right) = 0$ is clearly maintained, since we only have one component of the magnetic field, H_z, which is perpendicular to x–y plane and symmetry along z-direction is assumed.

3. Results and discussion

The present study aims at introducing a modified form of the FDTD equations for electromagnetics involving material motion, and its validation against analytical solutions. Another aim is to study the sensitivity of results to computational parameters such as the permittivity scaling factor. The application of this technique to real-life flux compression systems will be reported separately.

Hence, in this section, arbitrary parameters are chosen for material conductivity σ, velocity v and system dimensions so as to minimize the overall computational demand. These parameters, of course, meet the necessary conditions discussed in Section 2.

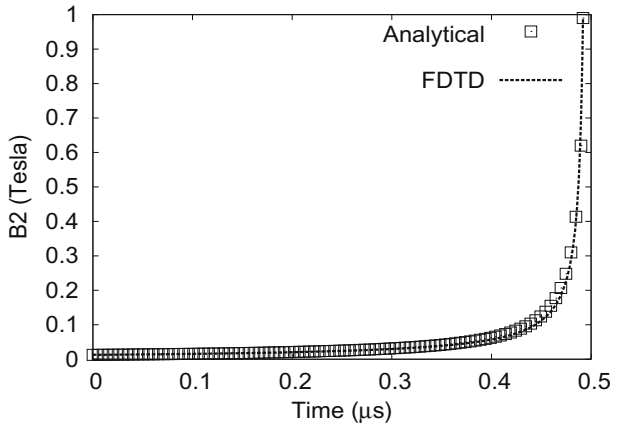

Fig. 5. Magnetic field inside the compression volume, B_2, as a function of time. Dotted curve is the analytical solution and solid line represents results from the FDTD calculation. $t = 0$ refers to the time when the source magnetic field reaches its peak value.

3.1. Results obtained by using Scheme-2

3.1.1. Case 1

As a first step, we have chosen a flux compression system similar to the one given in [5]. The initial magnetic field outside the compression volume is zero ($B_{10} = 0$), with a compression length of 50 mm in both x and y directions. The dimensions of the B10 region and thicknesses of walls are 20 mm and 1 mm respectively. The initial magnetic field inside the compression volume, B_{20} is 1.256×10^{-2} T. The total flux injected into the system is thus 3.14×10^{-5} T m^2 (Wb). The thickness and conductivity of slab are 10 mm and 1×10^6 S/m respectively. Cell-sizes are taken as $\Delta x = 0.1$ mm and $\Delta y = 1$ mm, leading to a problem size of 860×110 cells, including the distance to the boundary. A uniform velocity of 100 km/s in the positive x-direction is given to the slab when the field reaches its peak value B_{20}. This velocity lies in the range (20–400 km/s) offered by plasma armatures [5,33]. This implies $R_d \approx 251$. The permittivity of the medium is artificially increased by a factor of 100, relative to free space, to allow a larger time-step while satisfying all the constraints discussed in Section 2.

The temporal amplification of the initial magnetic field B_{20} due to flux compression, and the analytical solution given in [5], is shown in Fig. 5. Good agreement is observed.

A plot showing the normalized flux inside the system is shown in Fig. 6. The total flux is evaluated for the entire computational domain. It is clear that the total flux inside the system is conserved during the compression stage. A small decrease in the flux (≈0.02%) towards the end of operation is observed, which is in the acceptable range.

There is an induced electric field (motional EMF, $E_v = v_x B_z$) on the surface of the conductor moving across the magnetic field. The computed result is compared with analytical solutions given in [5] and reasonable agreement is found, as shown in Fig. 7.

The spatial variation of magnetic field inside the compression volume at three different times during the compression stage is shown in Fig. 8. Data points to the left of the flat-top, at any given time, show field diffusion into the moving conductor.

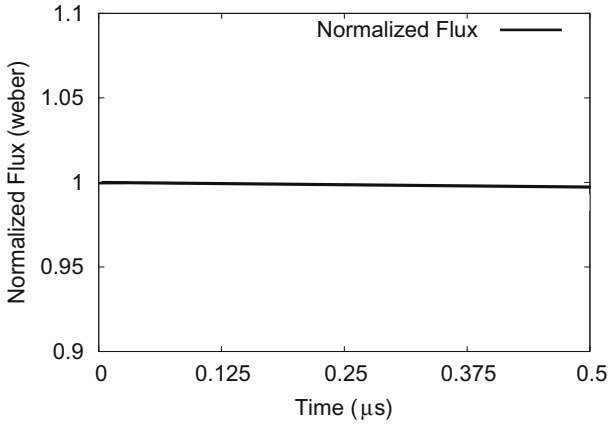

Fig. 6. Time history of normalized magnetic flux inside the system. The normalization factor is the initial flux in the system = 3.14×10^{-5} T m^2 (Weber).

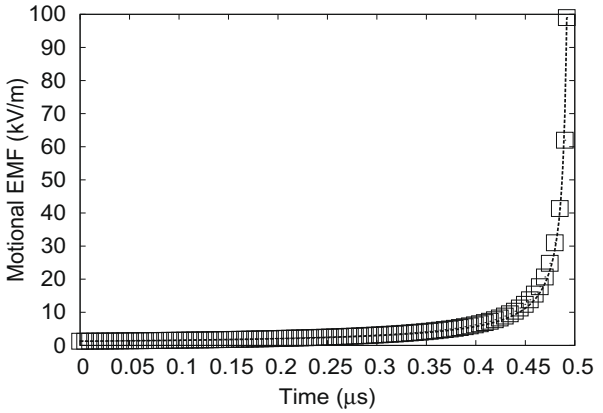

Fig. 7. Magnitude of induced EMF (kV/m) on the surface of the slab ($E_v = v_x \times B_z$). Both analytical and computed values are shown.

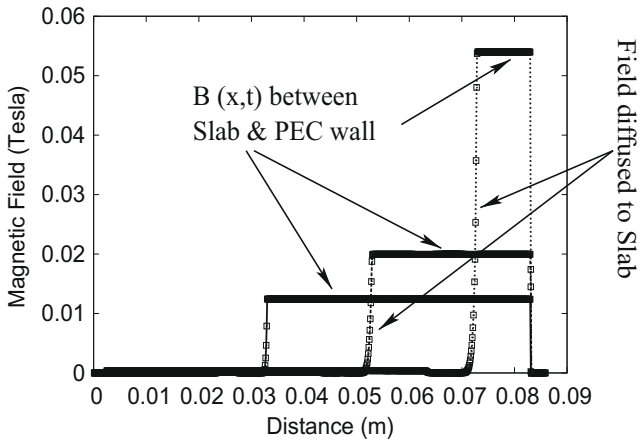

Fig. 8. Spatial variation of magnetic field inside the compression volume, illustrating field amplification. Three different plots correspond to field variations at three different times during compression. Points represent analytical solutions while line plots shows numerical results.

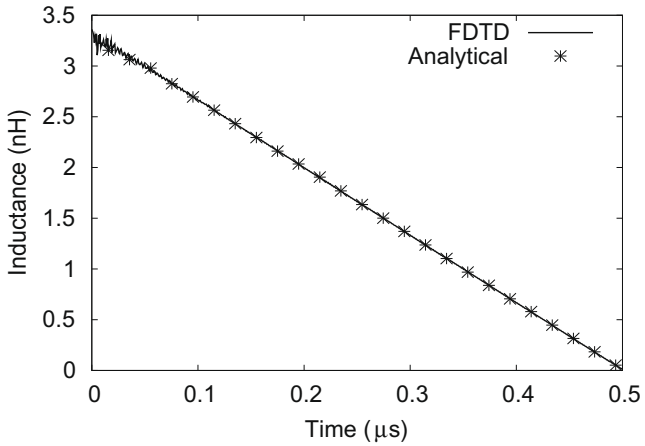

Fig. 9. Inductance as a function of time. Analytical and FDTD results match well.

The inductance per unit width in the z-direction, i.e., perpendicular to the plane of Fig. 3, can be calculated using Eq. (22).

$$L = \frac{\Phi_{total}}{I} = \frac{\int_s \vec{B} \cdot \vec{dS}}{I} \tag{22}$$

where I is the total current per unit width of the conductor, $\vec{dS}$ is an area element in the x–y plane and Φ_{total} is the total flux linked with the compression volume. Here, the total area $\vec{S}$ include only the compression volume. The variation of inductance with time is plotted in Fig. 9, along with analytical solutions from [1]. Good agreement can be seen.

3.1.2. Case 2

We next investigate a flux compression problem described in [4], where the field outside the compression volume B_{10} is non-zero. System dimensions and material parameters are the same as described in Section 3.1.1, with $B_{10} = 1.256 \times 10^{-3}$ T, i.e., 10% of B_{20}. The spatial variation of the magnetic field inside the compression volume at two different times during the compression is shown in Fig. 10. The FDTD results are found to be in good agreement with analytical results given in [4]. Fig. 11 shows the normalized magnetic fields inside $(B_2(t)/B_{peak})$ and outside $(B_1(t)/B_{10})$ the compression volume. Reasonable agreement between FDTD results and analytical solutions is observed.

3.1.3. Sensitivity to permittivity scaling factor

The permittivity of the medium is scaled-up artificially as in [9–11] to achieve higher time-step by meeting all the constraints mentioned in Section 2.2. However, it is important to observe the extent of scaling that can be achieved without introducing significant errors in physical quantities of practical interest, e.g., compressed magnetic field.

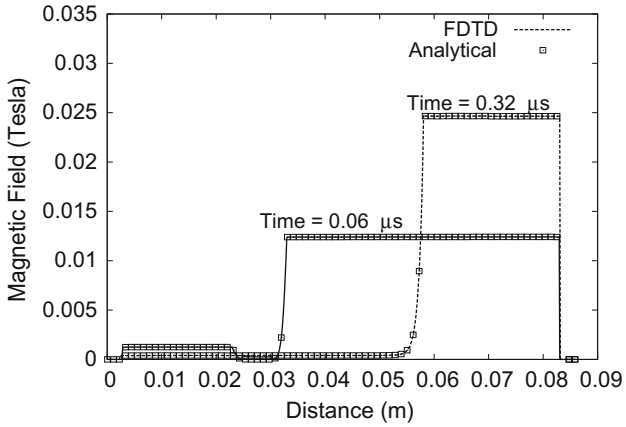

Fig. 10. Spatial variation of magnetic field inside the compression volume for Case-2. Dots and solid lines represent analytical and computational solutions, respectively.

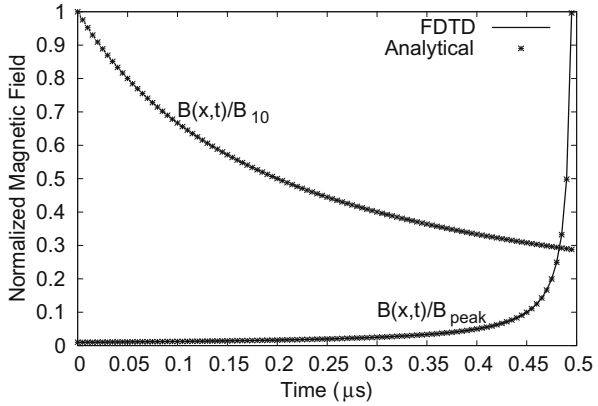

Fig. 11. Normalized magnetic fields inside $(B_2(t)/B_{peak})$ and outside $(B_1(t)/B_{10})$ the compression volume, as functions of time. B_{peak} is the peak magnetic field reached in the compression volume. Dots and solid lines represent analytical and computational solutions, respectively. $t = 0$ refers to the time when the source magnetic field reaches its peak, and conductor motion starts.

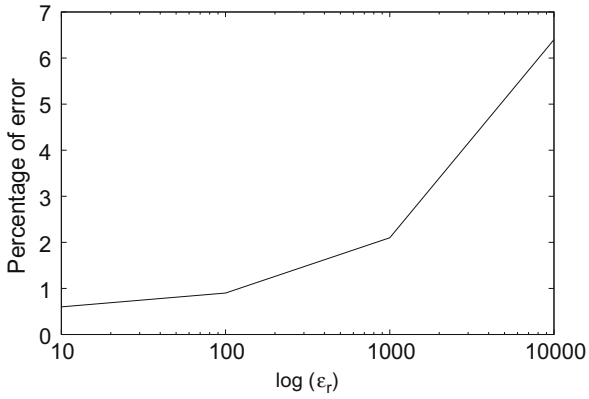

Fig. 12. Percentage error between analytical and numerical solutions, as a function of the permittivity scaling factor (ϵ_r).

Hence we next examine the sensitivity of computational results to the scaling factor used for the permittivity of free space, i.e., ϵ_r. We consider the problem described in [5], with system dimensions given in Section 3.1.1. The scaling factor

is varied from 10 to 10000. For each scaling factor, we compute the percentage difference between the analytical and numerical solutions for the magnetic field inside the compression volume at the end of the compression. Fig. 12 shows the result. For the case examined here, the overall error remains a few percent, although there is a monotonic increase with ϵ_r. Furthermore, the error only changes by a few percent for a change of three orders of magnitude in ϵ_r. Hence, while a higher ϵ_r would certainly help increase the time-step and reduce the computational load, it comes at the cost of reduced accuracy. Note also that this may significantly change for other system parameters where the diffusion scales are different.

The conclusion is that the acceptable scaling factor that can be used for achieving higher time-steps needs to be selected carefully, depending upon system parameters and the desired accuracy level.

3.1.4. Convergence test

Next, we have performed a convergence test by comparing analytical solutions and FDTD simulated results for different mesh-size. To investigate the sensitivity of mesh-size on the convergence of numerical results, a test problem mentioned in [5] with system dimensions given in Section 3.1.1 has been used with permittivity scaling factor equal to 100. The mesh-size is varied from 0.025 mm to 0.4 mm along the direction of velocity. The numerical error estimated is plotted against mesh-size, See Fig. 13. For the case examined here, the numerical results have converged with respect to the mesh-size ($\Delta x \approx 0.1$ mm). The variation of numerical error estimated with respect to permittivity scaling factor for different mesh-size shows similar trend as discussed in (3.1.3). The acceptable mesh-size may vary for different system parameters depending on conductivity (skin-depth), velocity, etc. Therefore, an acceptable mesh-size that can be used needs to be selected carefully, depending upon system parameters and the desired accuracy level.

3.2. Results obtained by using Scheme-1

A flux compression system with system dimensions described in Section 3.1.1 is used for this study. The magnetic field at two different times during compression stage is depicted in Fig. 14. The results are found to be oscillatory in nature.

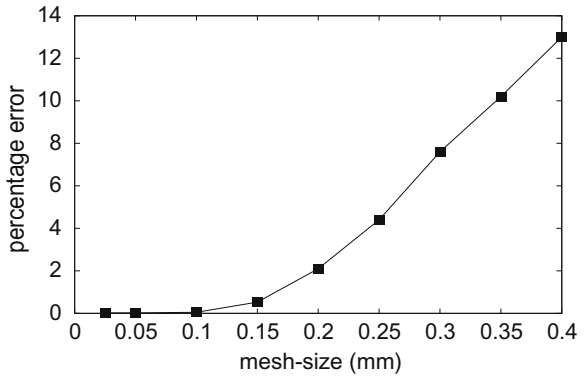

Fig. 13. Percentage error between analytical flux conservation factor and numerical solutions, as a function of mesh-size.

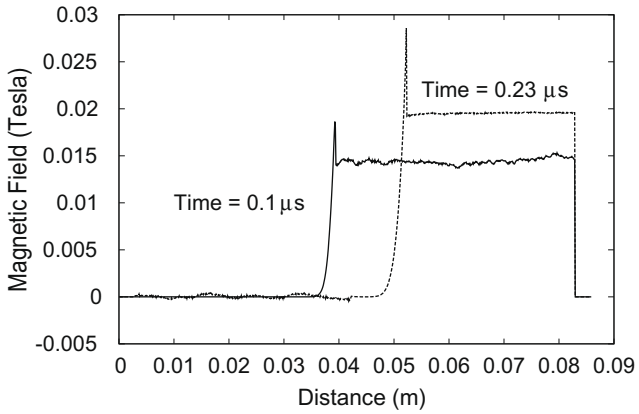

Fig. 14. Spatial variation of magnetic field inside the compression volume calculated by using Scheme-1. Different plots correspond to field variations at two different times during compression.

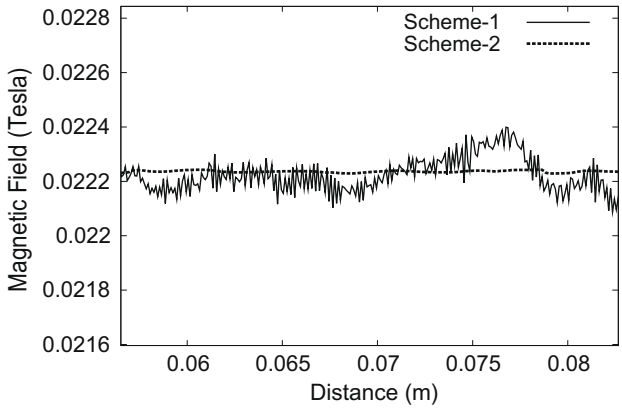

Fig. 15. A zoomed in plot for the comparison of spatial variation of magnetic field inside the compression volume calculated by two different methods namely, Scheme-1 and Scheme-2.

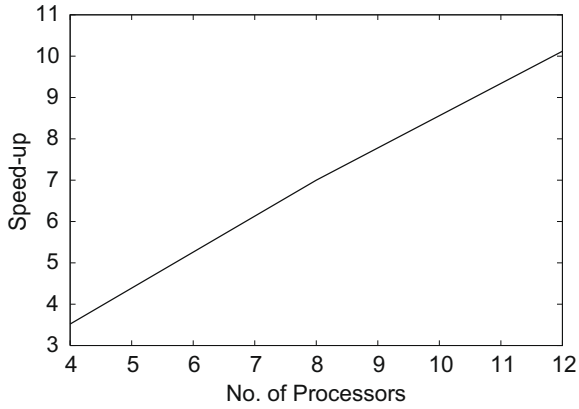

Fig. 16. Speedup achieved as a function of the number of processors, for the problem described in Section 3.1.1.

A comparison of the spatial variation of magnetic field obtained by using two different numerical schemes namely, Scheme-1 and Scheme-2 can be seen in a zoomed in plot shown in Fig. 15. It is clear from the figure that the results obtained by using Scheme-1 leads to ripples in the numerical solution.

We found that the direct addition of E_v in Eq. (2) leads to ripples in numerical solutions, especially near the boundaries of moving conductors, and these ripples then spread to the entire computational domain. However, this scheme conserve the total magnetic flux in the system.

3.3. Parallel computation

Even sample problems of the kind discussed above require a fairly large mesh. Simulations for practical flux compression problems would thus impose a much greater computational load. Hence it is important to examine the performance of a parallelized version of this algorithm on a parallel cluster.

The 2-D algorithm has been parallelized using message passing interface (MPI) [32] for communication between processors. The flux compression system mentioned in Section 3.1.1 requires a mesh-size of 860×110 in x and y directions respectively. Computer code performance has been studied on a 33 node, 3.0 GHz, Dual core, Dual Socket Xeon cluster with Infiniband interconnect. The speedup achieved as a function of the number of processors is shown in Fig. 16. It can be seen that the speedup varies approximately linearly with the number of processors used.

4. Limitations of the study

The present study suffers from the following major limitations. Firstly, it is extremely demanding in terms of computational power. Hence the work should be regarded as a first, exploratory step rather than as a mature technique ready for application to design. Secondly, the spatial variation of conductivity inside the conductor, due to effects like Joule heating,

has been neglected in the present work. It is, however, straightforward to include an arbitrary conductivity distribution consistent with Joule heating in the FDTD model.

5. Conclusions

The finite difference time domain (FDTD) method, adapted for magnetic field diffusion problems, has been applied to study electromagnetic induction in moving materials similar to magnetic flux compression systems. These simulations have been performed using a locally-developed two-dimensional variable-mesh FDTD code that has been parallelized along two directions. This technique allows the study of complex, multi-material configurations with arbitrary non-relativistic material velocity. The time domain analysis allows handling of arbitrary temporal waveforms of current. This technique thus allows a study of real-life configurations with practically no limitations on the geometric complexity, the materials used or the temporal waveforms. To our knowledge, this is the first application of this powerful technique to electromagnetic problems involving material motion.

However, the technique also suffers from the disadvantage of being extremely demanding in terms of computational power. Hence the present work should be regarded as a first, exploratory step rather than as a mature technique ready for application to design.

Acknowledgments

We thank the referees for their suggestions, which have helped to significantly improve the quality of the paper.

References

[1] C.M. Fowler, R.S. Caird, W.B. Garn, An Introduction to Magnetic Flux Compression Generators, LANL Report LA-5890-MS, 1975.
[2] John R. Freeman, Samuel L. Thompson, Numerical methods for studying compressed magnetic field generators, J. Comp. Phys. 25 (1977) 332–352.
[3] H.E. Wilhelm, Electromagnetic induction in accelerated conductors, Phys. Rev. E 25 (1982) 2913–2922.
[4] H.E. Wilhelm, Electromagnetic induction in accelerated conductors with frontal compression and rear dilution of magnetic flux, J. Appl. Phys. 58 (1984) 1285–1292.
[5] H.E. Wilhelm, Electromagnetic induction in conductors. Accelerated in magnetic field amplified by flux compression, Appl. Phys. B 31 (1983) 107–113.
[6] K.S. Kunz, R.J. Luebbers, The Finite Difference Time-Domain Method for Electromagnetics, CRC press, 1993.
[7] K.S. Yee, IEEE Trans. Anten. Propag. AP-14 (1966) 302–307.
[8] Richard Holland, Finite-difference time-domain (FDTD) analysis of magnetic diffusion, IEEE Trans. Electromagn. Comp. 36 (1) (1994) 32–39.
[9] Richard Holland, FDTD analysis of nonlinear magnetic diffusion by reduced *c*, IEEE Trans. Anten. Propog. 43 (7) (1995) 653–659.
[10] R. Holland, L. Simpson, K.S. Kunz, Finite-difference analysis of EMP coupling to lossy dielectric structures, IEEE Trans. Electromagn Comp. 22 (2) (1980) 203–209.
[11] C.D. Sijoy, Shashank Chaturvedi, Calculation of accurate resistance and inductance for complex magnetic coils using the finite-difference time-domain technique for electromagnetics, IEEE Trans. Plasma Sci. 36 (2008) 70–79.
[12] C.D. Sijoy, D. Sharma, S. Chaturvedi, Use of 3-D FDTD method for magnetic field diffusion calculations in complex pinch geometries, Presented at VIII Khariton Readings, RFNC-VNIIF, Russia, 2006.
[13] C.D. Sijoy, S. Chaturvedi, Three-dimensional calculations of electrical parameters in flux compression systems, in: International Conference on Megagauss Magnetic Field Generation and Related Topics, USA, 2006 (5–10 November).
[14] J.P. Boris, D.L. Book, Flux-corrected transport. I. SHASTA, a fluid transport algorithm that works, J. Comp. Phys. 11 (1973) 38–69.
[15] J.P. Boris, Flux-Corrected Transport Modules for Solving Generalized Continuity Equations, NRL Memorandum Report 3237, 1976.
[16] Allen Taflove, Susan C. Hagness, Computational Electrodynamics. The Finite-Difference Time-Domain Method, third ed., Artech House, Norwood, 2000.
[17] D. Sullivan, O. Gandhi, A. Taflove, Use of the finite-difference time-domain method for calculating EM absorption in man models, IEEE Trans. Biomed. Eng 35 (1988) 179–186.
[18] R.J. Speigal, M.B.E. Fatmi, K.S. Kunz, Application of a finite-difference technique to the human radiofrequency dosimetry problem, J. Microw. Power Electromagn. Energy 20 (1985) 241–254.
[19] H.J. Longley, C.L. Longmire, Development of the GLANC EMP Code, Defence Nuclear Agency, DNA3221T (December 1973).
[20] J.P. Berenger, A perfectly matched layer for the absorption of electromagnetic waves, J. Comput. Phys. 114 (October) (1994) 185–200.
[21] D.S. Katz, E.T. Thiele, A. Taflove, Validation and extension to three dimensions of the berenger PML absorbing boundary condition for FDTD meshes, IEEE Microw. Guided Wave Lett. 4 (August) (1994) 268–270.
[22] Peter G. Petropoulos, Analysis of exponential time-differencing for FDTD in lossy dielectrics, IEEE Trans. Anten. Propag. 45 (6) (1997) 1054–1057.
[23] C. Moon Francis, Magneto-Solid Mechanics, Wiley Interscience Publication, John-Wiley, New York, 1984.
[24] J.D. Jackson, Classical Electrodynamics, third ed., John Wiley and Sons Inc., New York, 1998.
[25] A. Harten, High resolution schemes for hyberbolic conservation laws, J. Comp. Phys. 49 (1983) 357.
[26] D. Ryu, F. Miniati, T.W. Jones, A. Frank, A divergence-free upwind code for multidimensional magnetohydrodynamic flows, Astro. Phys. J. 509 (December) (1998) 244–255.
[27] Gabor Toth, Dusan Odstrcil, Comparison of some flux corrected transport and total variation diminishing numerical schemes for hydrodynamic and magnetohydrodynamic problems, J. Comp. Phys. 128 (1996) 82–100.
[28] J.M. Stone, A radiation magnetohydrodynamics code for astrophysical flows in two space dimensions. I – The hydrodynamic algorithms and tests, Astrophys. J. Suppl. Series 80 (June) (1992) 791.
[29] S.T. Zalesak, Fully multidimensional flux-corrected transport algorithms for fluids, J. Comp. Phys. 31 (1979) 335–362.
[30] C.R. DeVore, Flux-corrected transport techniques for multidimensional compressible magnetohydrodynamics, J. Comp. Phys. 110 (1994) 310–319.
[31] G. Mur, Absorbing boundary conditions for the finite difference approximation of the time domain electromagnetic field equations, IEEE Trans. Elect. Compat. 23 (1981) 377.
[32] Marc Snir, MPI: The Complete Reference, 2nd ed., vol. 1, MIT Press, 1998.
[33] R.J. Litchford, G.A. Robertson, Magnetic Flux Compression Reactor Concepts for Spacecraft Propulsion and Power, NASA Tech. Report, NASA/TP-2001-210793, 2001.
[34] A. Sommerfield, Electrodynamics, Academic Press Inc., New York, 1952.